Fast Recovery of the High Work Function of Tungsten and Molybdenum Oxides via Microwave Exposure for Efficient Organic Photovoltaics

ARTICLE *in* JOURNAL OF PHYSICAL CHEMISTRY LETTERS · MAY 2014

Impact Factor: 7.46 · DOI: 10.1021/jz500612p

5 AUTHORS, INCLUDING:

Maria Vasilopoulou
National Center for Scientific Research Demok…
96 PUBLICATIONS **715** CITATIONS
SEE PROFILE

Panagiotis Argitis
National Center for Scientific Research Demok…
193 PUBLICATIONS **1,925** CITATIONS
SEE PROFILE

Thomas Stergiopoulos
Aristotle University of Thessaloniki
69 PUBLICATIONS **2,486** CITATIONS
SEE PROFILE

D. Davazoglou
National Center for Scientific Research Demok…
130 PUBLICATIONS **1,311** CITATIONS
SEE PROFILE

THE JOURNAL OF PHYSICAL CHEMISTRY Letters

Letter

pubs.acs.org/JPCL

Fast Recovery of the High Work Function of Tungsten and Molybdenum Oxides via Microwave Exposure for Efficient Organic Photovoltaics

Maria Vasilopoulou,* Anastasia Soultati, Panagiotis Argitis, Thomas Stergiopoulos, and Dimitris Davazoglou

Institute of Nanoscience and Nanotechnology (INN), NCSR "Demokritos", 153 10 Agia Paraskevi, Attiki, Greece

Supporting Information

ABSTRACT: In this work, we use microwave exposure of tungsten and molybdenum oxides to improve hole extraction in organic photovoltaics (OPVs). This is a result of fast recovery of the high work function of metal oxides occurring within a few seconds of microwave processing. Using the space-charge-limited current model, we verified the formation of an anode contact that facilitates hole extraction, while Mott−Schottky analysis revealed the enhancement of the device built-in field in the devices with the microwave-exposed metal oxides. Both were attributed to the formation of large interfacial dipoles at the ITO/microwave-exposed metal oxide interface. The power conversion efficiency (PCE) of OPVs using microwave-exposed metal oxides and based on blends of poly[(9-(1-octylnonyl)-9H-carbazole-2,7-diyl)-2,5-thiophenediyl-2,1,3-benzothiadiazole-4,7-diyl-2,5-thiophenediyl] (PCDTBT) with ([6,6]-phenyl-C_{71} butyric acid methyl ester, $PC_{71}BM$) reached values of 7.2%, which represents an increase of about 30% compared with the efficiency of 5.7% of devices using metal oxides not subjected to microwave exposure.

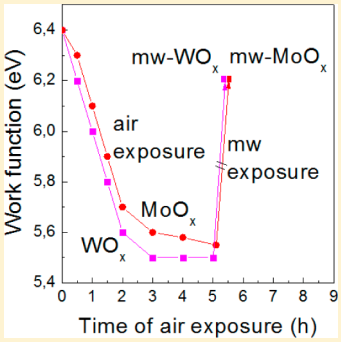

SECTION: Energy Conversion and Storage; Energy and Charge Transport

A substantial amount of research has been undertaken the last decades toward creating commercially viable organic photovoltaic (OPV) cells. This is due to the potential use of OPV cells as an inexpensive source of renewable energy.[1−6] As a result, reported efficiencies have increased rapidly and now exceed 10% in multijunction cells.[7,8] These efficiencies remain, however, well below the thermodynamic limit for single-junction organic solar cells, estimated to be >20%.[9] Thus, significant challenges and opportunities remain in optimizing energy conversion in OPV cells, which include improvements in photoactive layer materials to enhance photogeneration of charge carriers and careful tailoring of contacts and interlayer materials to facilitate charge collection and minimize recombination losses.[10−13] Because work function differences between anode and cathode contacts alone are not sufficient to ensure holes or electrons harvesting selectively at opposing contacts, additional interlayers for use between the photoactive materials and the electrodes were identified to be important and need to be developed to create this selectivity and optimize therefore cell performance.[14−22]

In recent years, intense work has been carried out on the modification of the anode contact using high work function transition-metal oxides, especially those of tungsten and molybdenum.[23−30] These metal oxides need to exhibit high work function (W_F) to reduce the barrier for hole extraction from the organic photoactive layer to the metallic anode through the formation of a large interfacial dipole.[24,31] However, it has been reported that air exposure substantially reduces their W_F values down to 5.2−5.4 eV due to oxygen/moisture adsorption and surface contamination.[32,33] Because many organic semiconductors have an ionization potential (IP) above 5.5 eV, an anode interlayer with such a low W_F would not be sufficient for good contact.[33] Up to now, the most effective strategy to recover the high work function of air-exposed tungsten and molybdenum oxide films is the conventional thermal annealing in ultrahigh vacuum (UHV) at temperatures around 560 °C and above.[34] However, in conventional annealing methods implementing thermal conduction, such as hot plates or ovens, the high temperature required, the energy loss, and the low efficiency of energy usage can be problematic. In addition, such metal oxides are wide band gap semiconductors, adding a large series resistance to the device. Recently, important research progress has been made on the use of under-stoichiometric metal oxides that exhibit occupied gap states the level of which can be adjusted near the energy level of the highest occupied molecular orbital (HOMO) of the donor in the photoactive layer in order to facilitate hole extraction.[35−39] Despite the fact that these under-stoichiometric metal oxides are sufficiently conductive, their work function also exhibits an undesirable shift toward lower values (on the order of 5.4−5.6 eV[24]).

Received: March 28, 2014
Accepted: May 13, 2014

   dx.doi.org/10.1021/jz500612p | J. Phys. Chem. Lett. 2014, 5, 1871−1879

In this work, we present an easy, cost-effective, and rapid process for the fast recovery of the work function up to 6.2 eV of air-exposed under-stoichiometric tungsten and molybdenum oxides via microwave annealing. Regarding the interaction of microwaves with metal oxides, it has been reported that the latter absorb microwave energy and convert it to heat.[40−42] In conventional heating, the thermal energy is transferred to the material from the outside to the inside, creating a temperature gradient. Microwave exposure overcomes this through absorption of the microwave energy throughout the volume of the material, which leads to improved electrical and optical properties upon microwave processing of metal oxide semiconductors.[43−45] Here, we present experimental evidence that a short microwave exposure of under-stoichiometric tungsten and molybdenum oxides, while not altering the metal oxides' stoichiometry and positioning of gap states, induces a shift of about 0.7 eV of the work function toward higher values, which can be probably attributed to the effective removal of adsorbed oxygen atoms and water molecules similarly to conventional heating. More importantly, by using these microwave-exposed metal oxides as anode interlayers, OPV cells based on PCDTBT:$PC_{71}BM$ blends were fabricated exhibiting efficiency as high as 7.2%, which is 30% improved compared with the efficiency of 5.7% of the cells with their metal oxide interlayers not subjected to the microwave processing. We also analyze current densities in hole-only devices and capacitance and transient photoluminescence measurements to probe the effect of microwave exposure of oxide interlayers in interfacial hole transport/extraction for the studied OPV devices.

The microwave-exposed tungsten (mw-WO_x) and molybdenum (mw-MoO_x) oxides were prepared with the following procedure. First, under-stoichiometric tungsten (WO_x) and molybdenum (MoO_x) oxides were deposited in a hydrogen-containing environment with a previously reported deposition method (more details are included in the Experimental Section),[35−39] which were then removed out of the deposition chamber and exposed to air for a few hours prior to their characterization and/or device fabrication. By using ultraviolet photoelectron spectroscopy (UPS), we found that the metal oxide films started with high initial W_F values equal to 6.4 eV but, with air exposure, the surface W_F gradually reduced to much lower values. This reduction was attributed to adsorption of oxygen and moisture on the metal oxide surface.[32] The relative humidity in the laboratory was about 30% during the air exposure, and the samples remained at room temperature. With air exposure, the surface W_F continuously decreased within the first few hours and was saturated at 5.5 eV for tungsten and at 5.6 eV for molybdenum oxide after 4−5 h (Figure S1, Supporting Information). Some of these samples were then subjected to microwave exposure at a heating power of 350 W for about 30 s to obtain the microwaved tungsten (mw-WO_x) and molybdenum (mw-MoO_x) oxides. Their surface W_F (and also stoichiometry and hydrogen content) was evaluated immediately after microwave exposure using UPS (and XPS) spectroscopy. It was found that, despite the fact that metal oxides remained under-stoichiometric with nearly the same degree of reduction and hydrogen content prior and after their microwave exposure (as derived from the analysis of the binding energy (BE) values of W 4f and O 1s peaks in the XPS spectra of tungsten oxides (Figure S2, Supporting Information) and of Mo 3d and O 1s in the XPS spectra of molybdenum oxides (Figure S3, Supporting Information)), their WF was significantly recovered during the 30 s of the microwave exposure. Figure 1 shows the UPS spectra of air-exposed for about 5 h under-stoichiometric tungsten (Figure 1 a) and

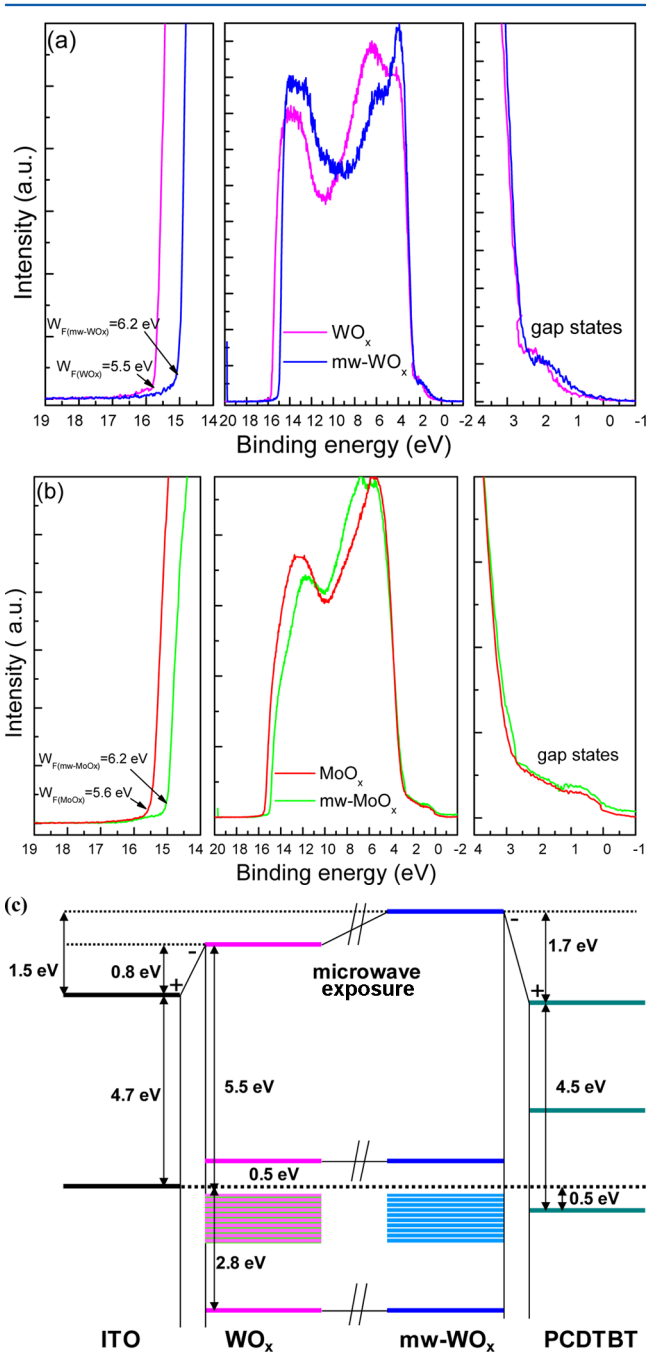

Figure 1. Secondary electron edge (left), valence band (middle), and near E_F region (right) of the UPS spectra of about 20 nm thick (a) WO_x and mw-WO_x and (b) MoO_x and mw-MoO_x films on ITO substrates. (c) The energy level diagram of the ITO/tungsten oxides/PCDTBT:$PC_{71}BM$ interfaces, as derived from UPS measurements.

molybdenum (Figure 1 b) oxide films, prior to and after their microwave exposure. In the left and right panels of these panels, the secondary electron edge of the UPS spectra and the near-Fermi level region, respectively, are shown. It can be seen that the UPS spectra of both tungsten and molybdenum oxides exhibit two main peaks that are slightly shifted after microwave exposure, evidence for slight transformations of the materials structure. All spectra also exhibit broad features near the Fermi

dx.doi.org/10.1021/jz500612p | J. Phys. Chem. Lett. 2014, 5, 1871−1879

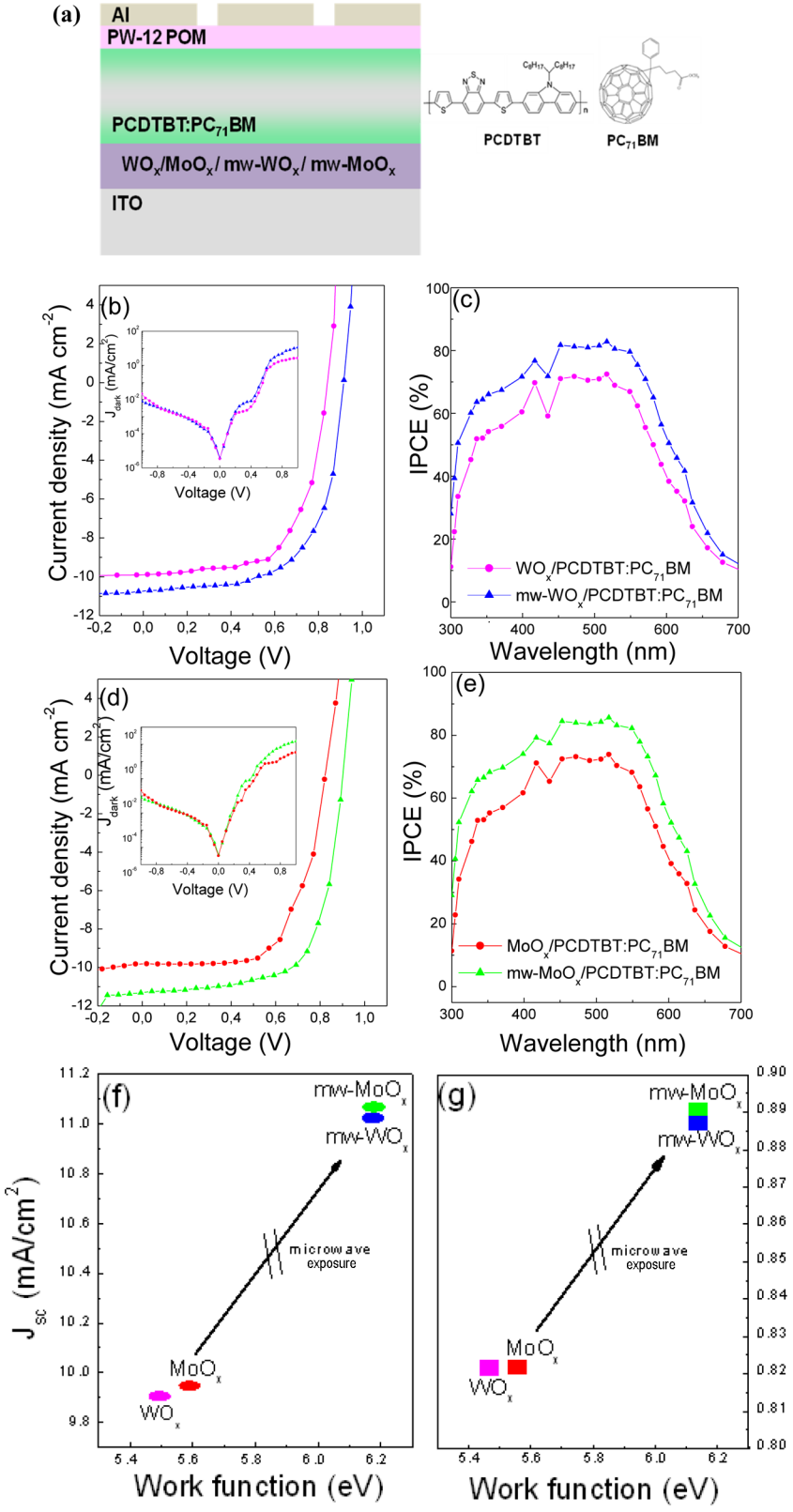

Figure 2. (a) Representative device architecture and structure of the organic semiconductors. (b) $J-V$ characteristics (with dark current curves shown as the inset) and (d) IPCEs of OPVs using PCDTBT:$PC_{71}BM$ as the photoactive layer and tungsten oxides as anode interlayers. (c) $J-V$ characteristics (with the dark current as the inset) and (e) IPCEs of devices using molybdenum oxides as anode interlayers. Variation of (f) J_{sc} and (g) V_{oc} with the work function changes of metal oxides for PCDTBT:$PC_{71}BM$-based devices.

level, indicative of new occupied states formed inside of the band gap with a relatively large density, which were attributed to the occupation of W 5d (in the case of tungsten oxides) or Mo 4d (for molybdenum oxides) orbitals with t_{2g} symmetry.[28,29] Note that the microwave exposure step does not alter the position and/or density of these states lying near the Fermi

dx.doi.org/10.1021/jz500612p | J. Phys. Chem. Lett. 2014, 5, 1871−1879

Table 1. Photovoltaic Properties and SCLC Data of the PCDTBT:$PC_{71}BM$-Based Devices with the Architecture ITO/WO_x, mw-WO_x, MoO_x, and mw-MoO_x (20 nm)/PCDTBT:$PC_{71}BM$ (150 nm)/PW-12 POM (5 nm)/Al[a]

metal oxide layer	J_{sc} (mA/cm^2)	V_{oc} (V)	FF	PCE (%)	μ_h (cm^2 V^{-1} S^{-1})
WO_x	**9.90**	**0.82**	**0.69**	**5.6**	3.62×10^{-5}
	9.80 (±0.10)	0.81(±0.01)	0.67(±0.02)	5.5(±0.1)	
mw-WO_x	**11.00**	**0.88**	**0.73**	**7.1**	3.86×10^{-5}
	10.90 (±0.10)	0.87(±0.01)	0.71(±0.02)	7.0(±0.1)	
MoO_x	**9.95**	**0.82**	**0.70**	**5.7**	6.87×10^{-5}
	9.85 (±0.10)	0.81(±0.01)	0.68(±0.02)	5.6(±0.1)	
mw-MoO_x	**11.05**	**0.89**	**0.73**	**7.2**	6.92×10^{-5}
	10.95 (±0.10)	0.88(±0.01)	0.71(±0.02)	7.1(±0.1)	

[a]Data and statistics based on 32 cells of each type. Numbers in bold are the maximum recorded values.

level (and also the value of energy gap, Figures S4 and S5 (Supporting Informaion)), which is of high significance beause these states may act as favorable paths for charge transport, allowing thus the charge carriers to be transported within the device. The most striking difference of the UPS line shape between the microwave-exposed metal oxides versus the ones not subjected to microwave processing (irrespective of the metal cation) is the positioning of the secondary electron edges of the UPS spectra, which are used to estimate the oxide's work function (W_F). The work function values of the air-exposed WO_x and MoO_x are estimated to be approximately 5.5 and 5.6 eV, respectively. After microwave exposure for 30 s, however, the W_F's of these films are shifted toward higher values, reaching the high value of 6.2 eV, which is close to the values of our freshly deposited metal oxides (Figure S1, Supporting Informaion). The fast and significant increase of the W_F of the microwaved W and Mo oxide films is expected to have a positive impact on the device performance because it could allow both the favorable energy level alignment at the anode contact through the formation of a large dipole with the appropriate direction (with its positive pole pointing toward the anode contact) and also beneficial charge transport via the gap states located near the Fermi level (which are not altered by the microwave exposure).[24,25] The energy level diagram for indium tin oxide (ITO)/WO_x or mw-WO_x/PCDTBT interfaces are depicted in Figure 1 c (the energy diagram for the ITO/molybdenum oxides interface is quite similar and omitted to avoid duplication). The ITO W_F was measured to be about 4.7 eV (not shown here). An interface dipole of 0.8 eV can be observed at the ITO/WO_x interface (beause the W_F of air-exposed WO_x is 5.5 eV, while the top of its valence band (VB) is located at 2.8 eV below the Fermi level and the position of the bottom of its conduction band (CB) at 0.5 eV is above the E_F as derived taking into account the measured optical band gap of the oxide, Figure S4 (Supporting Informaion)). Gap states are present just below the Fermi level of the under-stoichiometric WO_x film and are aligned with the HOMO of the PCDTBT (the UPS spectrum of a PCDTBT film is shown in the Supporting Informaion, Figure S6). With a short exposure to the microwave irradiation, a strong W_F recovery up to 6.2 eV of the mw-WO_x is observed. As a result, a large dipole of 1.5 eV is formed at the ITO/mw-WO_x interface, while the rest of the electronic structure of the interface remains unchanged. The energy diagram suggests that microwave annealing strongly enhances energy level alignment and interfacial dipoles without affecting the gap states and is, therefore, expected to have a beneficial impact on device operation.

Figure 2 a shows the device architecture and also the structure of the organic semiconductors studied here, where under-stoichiometric tungsten or molybdenum oxides, microwave-treated or not, taken from the same batches used for the UPS measurements, were used to facilitate the photogenerated holes' extraction from the HOMO of PCDTBT toward the ITO anode while a solution-processed PW12-POM layer was used to extract the photogenerated electrons from $PC_{71}BM$ to the Al cathode.[46,47] In Figure 2b and d, the current density versus voltage ($J-V$) characteristics of the OPV devices under AM 1.5 G illumination (using either microwave-exposed or not metal oxide anode interlayers) are presented. The $J-V$ characteristic curves under dark are also shown as insets. A tabular presentation of all cell operational characteristics, in particular, open-circuit voltage (V_{oc}), short-circuit current (J_{sc}), fill factor (FF), and PCE (with their statistics), is given in Table 1. In Figure 2c and e, the corresponding incident photon-to-electron conversion efficiencies (IPCEs) are also presented. The device based on WO_x exhibits a $J-V$ characteristic from which a PCE of about 5.6% is estimated, as a result of a J_{sc} of 9.90 mA cm^{-2}, a V_{oc} of 0.82 V, and a FF of 0.69 V. Similarly, the device with the MoO_x anode interlayer exhibits a PCE of 5.7% (J_{sc} = 9.95 mA cm^{-2}, V_{oc} = 0.82 V, and FF = 0.70 V). Upon subjecting the metal oxide interlayers to microwave exposure prior to the active layer deposition, the $J-V$ characteristics of the devices are significantly improved. In particular, the efficiency of the OPV cells with the mw-WO_x layer rises up to 7.1% as a result of the improved J_{sc}, V_{oc}, and FF (J_{sc} = 11.00 mA cm^{-2}, V_{oc} = 0.88 V, and FF = 0.73 V). Similar results were obtained for OPVs embedding the mw-MoO_x layers, which exhibit the high efficiency of 7.2% resulting from a J_{sc} of 11.05 mA cm^{-2}, a V_{oc} of 0.89 V, and a FF of 0.73 V, highlighting the impact of a short microwave exposure of the metal oxide layer in achieving efficient device operation. In addition, the dark $J-V$ curves of the devices with the microwave-exposed interlayers exhibit a higher forward current at all voltages and increased slope, indicating a decreased series resistance, R_s, and consequently a better anode contact compared with those of the corresponding devices with the unprocessed interlayers (Figure 2a and c, insets). It is reasonable then to suggest that the large interfacial dipoles formed between the microwave-exposed metal oxides and the PCDTBT:$PC_{71}BM$ active layer are at the origin of the improved anode contact in our devices, thus improving significantly the hole extraction/transport and consequently V_{oc} and FF. Figure 2c and e compares the IPCE spectra of the above devices. Both devices with the microwave-exposed metal oxide layers show high IPCE values (~83%) almost over the entire wavelength range, while the devices with the untreated

layers exhibit lower IPCE values (average of ~67%). Note that the spectral shape almost remains unchanged after microwave exposure, indicating that the enhanced photocurrent is due to the improved interfacial charge extraction/transport. This enhancement in IPCEs of devices using the microwave-exposed metal oxide layers can also explain the improvement of the measured photocurrent, which cannot be considered as a result of the improved extraction discussed above. The small but appreciable increase of the optical absorption of the active layer deposited on the microwave-treated metal oxides (Figure S7a, Supporting Information), which probably indicates that a change in the active layer thickness (also related to the observed increase of IPCEs) could be the origin of this improvement in J_{sc}. Furthermore, it is possible that the microwave exposure has sintered our metal oxide layers, thus altering their optical spacing capabilities, which could also increase the J_{sc}. From all of these results, it becomes evident that the microwave exposure of the metal oxide interlayers is highly critical for optimal solar cell performance, as illustrated in Figure 2f and g, where the J_{sc} and V_{oc} values of the devices based on PCDTBT:$PC_{71}BM$ with the change of the metal oxides W_F by the microwave processing are plotted. These results provide unambiguous evidence for the significant role of microwave exposure in recovering the high work function of the metal oxides and improve the solar cell performance in a fast, easy, and low energy-consuming manner.

To further characterize hole transport in our devices, we have performed space-charge-limited current (SCLC) measurements on hole-only devices using the device architecture ITO (anode)/metal oxide (20 nm)/PCDTBT:$PC_{71}BM$ (150 nm)/Au (cathode). The gold cathode causes a large barrier for electron injection/extraction to/from the LUMO of $PC_{71}BM$ from/to the electrode, and therefore, the resulting current is expected to be dominated by holes. In Figure 3a and b, the corresponding $J-V$ characteristics of the devices are shown on a log−log scale. From the $J-V$ characteristics, it is evident that in the low-voltage region, the current density increases when the metal oxide layer is subjected to the microwave exposure, indicating that hole transport becomes easier in the devices with the mw-WO_x/mw-MoO_x.

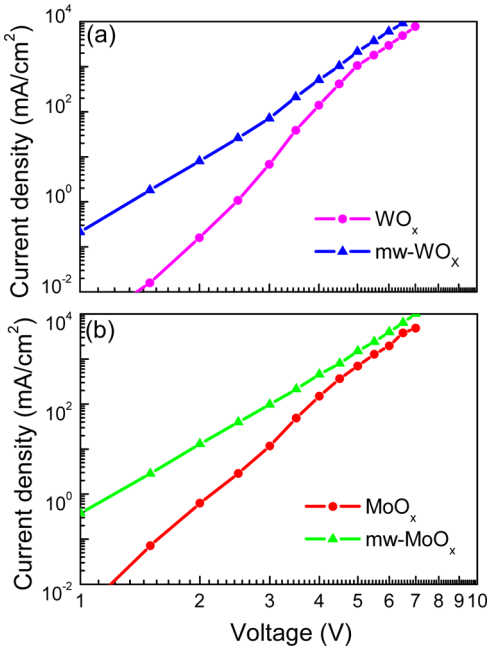

Figure 3. Room-temperature current−voltage curves on a log−log plot for PCDTBT:$PC_{71}BM$ hole-only devices exhibiting the structure ITO/metal oxides/PCDTBT:$PC_{71}BM$/Au, where the metal oxide layer is one of the (a) tungsten and (b) molybdenum oxides used in this study. The device active layers are all ~150 nm in thickness.

We have analyzed our hole-only devices using a SCLC model to fit the experimental results. Hole-only currents in disordered organic semiconductors are commonly modeled using analogues of Child's Law,[48,49] which describes single carrier currents in a trap-free insulator and predicts that the current density (J) varies by the square of the applied bias (V) and inversely by the cube of the film thickness (L) according to eq 1

$$J = \frac{9\varepsilon_o\varepsilon_r\mu_h V^2}{8L^3} \quad (1)$$

where $\varepsilon_o\varepsilon_r$ is the dielectric permittivity and μ_h is the hole mobility of the active layer. Note that to include the electric field dependency of the mobility, eq 1 can be appropriately modified according to the Mott−Gurney law (eq 2)

$$J = \frac{9\varepsilon_o\varepsilon_r\mu_{h,0} V^2 \exp[0.89\beta(V/L)^{1/2}]}{8L^3} \quad (2)$$

where $\mu_h = \mu_{h,0}\exp[\beta(V/L)^{1/2}]$ (Poole−Frenkel mobility law), $\mu_{h,0}$ is the zero-field mobility, and β is the field activation factor of the mobility. From Figure 3, the calculated hole mobility is enhanced in devices with the microwave-exposed metal oxide layers. The calculated hole mobilities were 3.62×10^{-5} and 3.86×10^{-5} cm^2 V^{-1} s^{-1} for the devices with the WO_x and MoO_x interlayers, respectively. These values increased to 6.87×10^{-5} and 6.92×10^{-5} cm^2 V^{-1} s^{-1} for the devices using the mw-WO_x and mw-MoO_x interlayers, respectively. Finally, the formation of a better contact at the anode interface for the devices with the microwave-exposed metal oxides can also be observed at low voltages and attributed to the perfect energy level alignment due to both the formation of a large favorable interfacial dipole and the occupation of gap states near the Fermi level.

The influence of microwave exposure of metal oxide layers on the device operation was further supported by the capacitance−voltage ($C-V$) measurements obtained in the PCDTBT:$PC_{71}BM$-based OPV cells shown in Figure 4a. $C-V$ measurements in devices based on organic semiconductors usually exhibit Mott−Schottky characteristics and can be used to obtain the built-in voltage (V_{bi}) of the device. In Figure 4b, the Mott−Schottky characteristics are shown, as derived from the $C-V$ measurements of the OPV cells embedding the metal oxides used in this study by using eq 3

$$C^{-2} = \left(\frac{2}{q\varepsilon N}\right)(V_{bi} - V) \quad (3)$$

where ε is the permittivity of the blend, N is the doping level, and q is the elementary charge.[50] The built-in voltage can be estimated from the intercept of the linear part of the curve with the voltage axis, while the doping level is from the $C^{2-}-V$ slope. From Figure 4b, it can be deduced that OPV cells fabricated on metal oxides not subjected to microwave exposure exhibit lower V_{bi} compared with their counterparts bearing the microwave-treated metal oxide bottom electrodes. This increase in V_{bi} (from 0.78−0.79 to 0.87−0.88 V) matches with the increase in the measured V_{oc} of the OPV devices. Regarding the origin of

dx.doi.org/10.1021/jz500612p | J. Phys. Chem. Lett. 2014, 5, 1871−1879

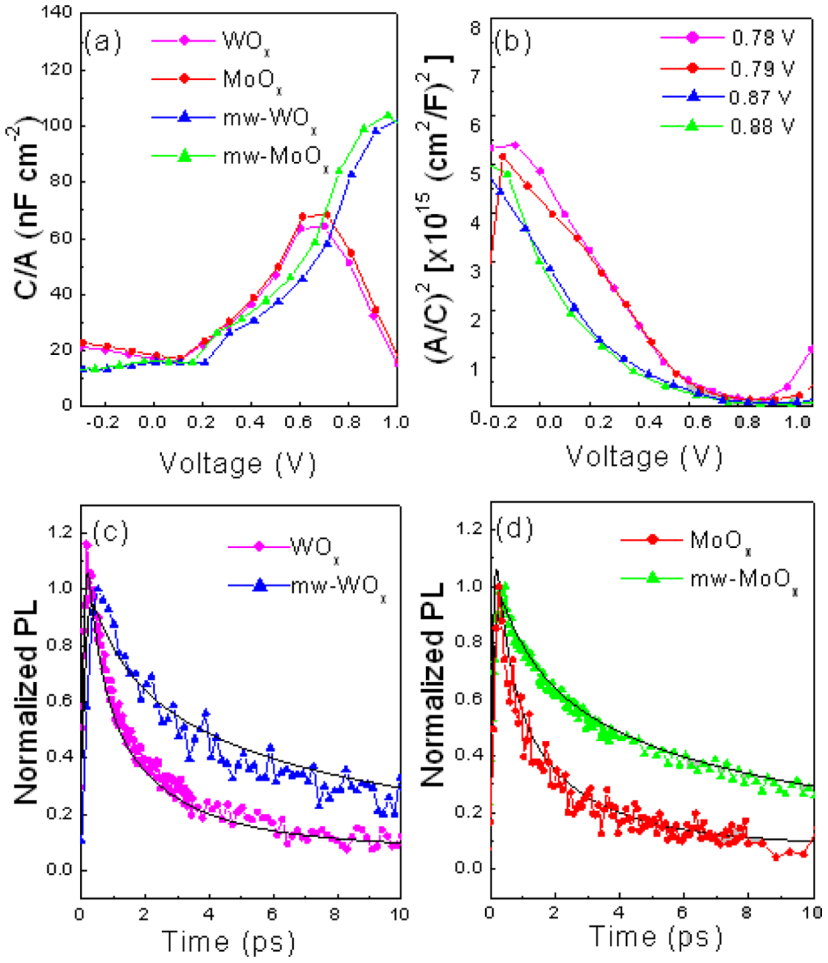

Figure 4. (a) Capacitance versus voltage ($C-V$) measurements of the PCDTBT:$PC_{71}BM$-based OPV devices. (b) Mott–Schottky characteristics of the OPV cells, exhibiting a linear relationship (straight lines) at low forward bias. The built-in potential V_{bi} is indicated for each curve. PL decay rates, detected at 710 nm PCDTBT:$PC_{71}BM$ films on microwave-exposed or not metal oxide layers used in this study: (c) on tunsgen oxides; (d) on molybdenum oxides.

the built-in voltage, it could be explained as follows: in a device incorporating no interlayers between the active layer and the metal electrodes, the built-in potential (which is equivalent to V_{bi}) is equal to the work function difference of the metal contacts. However, in the devices with modified electrodes by using appropriate interlayers, the built-in potential depends on the W_F of the interlayers. In our devices, the work function difference between the Al cathode and the metal-oxide-modified anode is related to the built-in potential as $V_{bi} = \Phi_{ox} - \Phi_{Al}$. Consequently, the increase in the W_F of the metal oxide anode interlayers after microwave processing can explain the higher V_{bi} estimated in the corresponding devices. Such an increase in the V_{bi} of the devices having their metal oxide layers subjected to microwave exposure is clear evidence of the interfacial electric field strengthening resulting in the observed enhancement of the hole transport/extraction rates.

Finally, in order to examine if microwave exposure of the metal oxide layers has a distinct effect on the exciton quenching, we employed femtosecond time-resolved PL spectroscopy. Figure 4c and d shows the normalized fluorescence dynamics at the emission peak of 710 nm (i.e., close to the wavelength of the active layer emission peak, Figure S6a (Supporting Information)) taken in the PCDTBT:$PC_{71}BM$ films deposited on top of the metal oxide layers upon excitation at 400 nm. The charge carrier lifetimes can be obtained by fitting the decay curves with a three-exponential equation of the form

$$f(t) = \sum_{i=1}^{3} A_i \exp\left(-\frac{t}{\tau_i}\right) \tag{4}$$

convoluted with the instrument's response function, which is considered to have a Gaussian profile. The amplitude-averaged lifetime is then determined by the equation

$$\langle\tau\rangle = \frac{\sum_{i=1}^{3} A_i\tau_i}{\sum_{i=1}^{3} A_i} \tag{5}$$

where A_i are the pre-exponential factors and τ_i are the three distinct time constants. All fitting parameters are summarized in Table 2. As shown in Figure 4c and d, the fluorescence decay rates of PCDTBT:$PC_{71}BM$ deposited on top of metal oxide layers were always lower when these layers were subjected to microwave exposure prior to organic layer deposition, suggesting corresponding increases in carriers' lifetimes (while the steady-state PL intensities of the organic films remained nearly unaffected, as is shown in Figure S6b (Supporting Information)). The measured increases in carrier lifetimes indicate more efficient exciton dissociations, which are probably

dx.doi.org/10.1021/jz500612p | J. Phys. Chem. Lett. 2014, 5, 1871–1879

Table 2. Multiexponential Fitting Parameters for the Fluorescence Dynamics of the PCDTBT:$PC_{71}BM$ Films on Microwaved or Not Metal Oxide Films with Excitation at 400 nm and Detection at 710 nm

metal oxide substrate	A_1	τ_1 (ps)	A_2	τ_2 (ps)	A_3	τ_3 (ps)	$\langle\tau\rangle$ (ps)
WO_x	0.48	0.56	0.29	4.5	0.23	16	5.3
mw- WO_x	0.7	1.70	0.99	10.6	0.15	28	10.4
MoO_x	0.53	1.00	0.2	4.0	0.27	15	5.4
mw-MoO_x	0.96	2.00	0,78	12	0.26	46	11.4

attributed to suppressed recombination losses in the devices using the microwave-treated metal oxides.[51,52]

In conclusion, we show here that we can effectively and quickly recover the high work function of tungsten and molybdenum oxides by a simple and short microwave exposure step. The net result of this work function recovery is the formation of large interfacial dipoles at the ITO/metal oxide/active layer interfaces, which have a crucial impact on the device operation because they enhance the transport/extraction of holes and may also suppress recombination losses at the anode contact. The PCE of OPVs using microwave-exposed metal oxides as anode interlayers and PCDTBT:$PC_{71}BM$ active layers reached values of 7.2%, which is 30% increased compared with the efficiency of 5.7% of devices using microwave-treated metal oxides. The microwave treatment presented here is, in the authors' knowledge, the simplest method for the recovery of the high work function of transition-metal oxides reported so far.

EXPERIMENTAL SECTION

Metal Oxide Preparation. Under-stoichiometric tungsten (WO_x) and molybdenum (MoO_x) oxides were deposited using a previously reported hot-wire vapor deposition system[28−30] by heating a metallic filament in a hydrogen-containing environment. The samples were positioned on an aluminum susceptor, 2.5 cm below a W/Mo filament (the diameter of the filaments was 0.5 mm, and they were purchased from Sigma-Aldrich), which was heated at 560 °C by a (AC) current flowing through two Cu leads. After loading the substrate, the reactor was evacuated down to 10^{-4} Torr. A PC-driven needle valve allowed the flow of forming gas (FG, a gas mixture containing 10% hydrogen and 90% nitrogen) through the reactor. Hot-wire W/Mo oxide films were then deposited by heating the corresponding metallic filament. The thickness of the films was controlled by changing the deposition time and taking into account the deposition rate, which was found to be about 0.25 nm/s. During deposition, the substrates remained near room temperature, depending on the deposition time, but without exceeding 50 °C. Then, all films were removed from the deposition chamber and exposed to air for several hours in order to adsorb oxygen and moisture, which reduce their initially high work function values.[32] Some of these air-exposed samples were transferred to a microwave oven (BP110 laboratory-grade microwave) employing a cavity magnetron, which generates rf radiation at a nominal frequency of 2.45 GHz and a heating power level of typically 300−1000 W. The heating power was set at 450 W, while the time of annealing was varied from a few seconds to several minutes. It was found that the desired work function shift to higher values was completed at about 30 s.

Device Fabrication and Characterization. OPV devices were fabricated on ITO-coated glass substrates (2 × 2 cm^2) with a sheet resistance of 20 Ω/square, which served as the anode electrode. Substrates were ultrasonically cleaned with standard solvents (15 min in deionized water, acetone, and isopropanol successively). An under-stoichiometric W or Mo oxide layer about 20 nm thick was deposited on top of ITO to serve as the anode interlayer, followed by an approximately 150 nm photoactive layer. The active layer consisted of a PCDTBT:$PC_{71}BM$ blend (both purchased from Sigma-Aldrich and used as received) with a 1:4 wt % ratio with a concentration of 25 mg/mL in chlorobenzene solution, and it was spin-cast on top of the metal oxide layer at 900 rpm. After spin coating, the active layer was annealed at 70 °C for 5 min in air. Then, a ∼5 nm tungsten polyoxometalate (12-phosphotungstic acid, $H_3PW_{12}O_{40}$, " PW-12 POM") film was spin-coated from a methanol solution to serve as the electron-selective interlayer. The devices were completed with a 150 nm thick aluminum top electrode, deposited in a dedicated chamber. All chemicals were purchased from Sigma-Aldrich and used with no further purification.

Measurements and Instrumentation. The film thickness was estimated with ellipsometry. Current density−voltage characteristics of the fabricated solar cells were measured with a Keithley 2400 source-measure unit. For V_{oc} and photocurrent measurements, devices were illuminated with a xenon lamp and an AM1.5G filter to simulate solar light illumination conditions with an intensity of 100 mW/cm^2. To accurately define the active area of all devices, we used aperture masks during the measurements, with their area equal to those of the Al contacts (12.56 mm^2). The capacitance−voltage measurements were recorded on devices exhibiting the same architecture as those described above (OPVs) at a frequency of 100 kHz and an AC bias of 25 mV by using a Keithley 4200-SCS DC characterization system. The measurements were performed in air at room temperature. The PL dynamics of the samples were studied by using time-resolved fluorescence upconversion spectroscopy in the femtosecond to picosecond time scale. The laser source was a mode-locked Ti:sapphire laser emitting 80 fs pulses at 800 nm with an 80 MHz repetition rate. The laser beam had been frequency-doubled through a BBO crystal, and the second harmonic at 400 nm was used as the excitation beam. The excitation power was kept below 5 mW. The PL of the samples was collected and focused together with the delayed fundamental laser beam (gate beam) on a second BBO crystal where an upconversion beam was generated (type-I phase matching). The upconversion beam passed through appropriate filters and a monochromator and was detected via a photomultiplier. All dynamics were detected under magic angle conditions. Chemical analysis of all metal oxide films (the freshly deposited, during air exposure, before and after microwave exposure) was performed with XPS measurements in an UHV VG ESCALAB210. The spectra were obtained after excitation using Mg Kα (1,253.6 eV) radiation of a twin anode in a constant analyzer energy mode with a pass energy of 30 eV. All binding energies were referred to the C 1s peak at 284.8 eV and to the O 1s peak at 530.2 eV of the surface adventitious carbon and oxygen, respectively. The W and Mo oxide stoichiometry was estimated using the XPS-measured W 4f and Mo 3d core levels, respectively, and the corresponding O 1s core-level spectra. To this extent, the areas under the photoemission peaks were integrated by fitting the O 1s and W 4f (or Mo 3d) spectra with asymmetric Gaussian−Lorentzian

dx.doi.org/10.1021/jz500612p | J. Phys. Chem. Lett. 2014, 5, 1871−1879

curves. The hydrogen content was estimated by fitting the O 1s core levels. The raw data, after a Shirley background subtraction, were fitted by a nonlinear least-squares routine using peaks with a mix of Gaussian−Lorentzian shape. The error is estimated at ±10% in all of the XPS-derived atomic percentages. The VB spectra of the metal oxides were evaluated after recording the UPS spectra of about 20 nm thick films deposited on an ITO substrate, taken from the batch used for OPV cell fabrication. For the UPS measurements, the He I (21.22 eV) excitation line was used. A negative bias of 12.28 V was applied to the samples during UPS measurements in order to separate sample and analyzer high BE cutoffs and estimate the absolute work function value from the high BE cutoff region of the UPS spectra. The analyzer resolution was determined from the width of the Au Fermi edge to be 0.16 eV. Because the high-intensity UV photons used for UPS measurements may alter the surface of metal oxide films, we adopted a certain protocol for the measurement of the oxides' work function; we first measure the core levels and work function of the sample using the low-intensity X-rays, then we measure the work function with the UPS, and finally, we measure again the core levels and work function with XPS to verify that the samples have remained unaffected.

■ ASSOCIATED CONTENT

Supporting Information

Additional figures (XPS, UPS, tauc plots, absorption, and steady-state photoluminescence spectra) are included (Figures S1−S7). This material is available free of charge via the Internet at http://pubs.acs.org.

■ AUTHOR INFORMATION

Corresponding Author

*E-mail: mariva@imel.demokritos.gr.

Notes

The authors declare no competing financial interest.

■ ACKNOWLEDGMENTS

This research has been cofinanced by the European Union (European Social Fund − ESF) and Greek national funds through the Operational Program "Education and Lifelong Learning" of the National Strategic Reference Framework (NSRF) - Research Funding Program: ARCHIMEDES III.

■ REFERENCES

(1) Tang, C. W. 2-Layer Organic Photovoltaic Cell. *Appl. Phys. Lett.* **1986**, *48*, 183−185.

(2) Yu, G.; Gao, J.; Hummelen, J. C.; Wudl, F.; Heeger, A. J. Polymer Photovoltaic Cells: Enhanced Efficiencies via a Network of Internal Donor−Acceptor Heterojunctions. *Science* **1995**, *270*, 1789−1791.

(3) Clarke, T. M.; Durrant, J. R. Charge Photogenaration in Organic Solar Cells. *Chem. Rev.* **2010**, *110*, 6736−6767.

(4) Kim, J. Y.; Lee, K.; Coates, N. E.; Moses, D.; Nquyen, T. Q.; Dante, M.; Heeger, A. J. Efficient Tandem Polymer Solar Cells Fabricated by All-Solution Processing. *Science* **2007**, *317*, 222−225.

(5) Gan, Q.; Bartoli, F. G.; Kafafi, Z. H. Plasmonic-Enhanced Organic Photovoltaics: Breaking the 10% Efficiency Barrier. *Adv. Mater.* **2013**, *25*, 2385−2396.

(6) Li, G.; Shrotriya, V.; Huang, J.; Yao, Y.; Moriarty, T.; Emery, K.; Yang, Y. High-Efficiency Solution Processable Polymer Photovoltaic Cells by Self-Organization of Polymer Blends. *Nat. Mater.* **2005**, *4*, 864−868.

(7) Green, M. A.; Emery, K.; Hishikawa, Y.; Warta, W.; Dunlop, E. D. Solar Cell Efficiency Tables (Version 40). *Prog. Photovoltaics* **2012**, *20*, 606−614.

(8) Green, M. A.; Emery, K.; Hishikawa, Y.; Warta, W.; Dunlop, E. D. Solar Cell Efficiency Tables (Version 41). *Prog. Photovoltaics* **2013**, *21*, 1−11.

(9) Bredas, J.-L. When Electrons Leave Holes in Organic Solar Cells. *Science* **2014**, *343*, 492−493.

(10) Janssen, R. A. J.; Nelson, J. Factors Limiting Device Efficiency in Organic Photovoltaics. *Adv. Mater.* **2013**, *25*, 1847−1858.

(11) Gargi, D.; Kline, R. J.; DeLongchamp, D. M.; Fisher, D. A.; Toney, M. F.; O'Connor, B. T. Charge Transport in Highly Face-On Poly(3-hexylthiophene) Films. *J. Phys. Chem. C* **2013**, *117*, 17421−17428.

(12) Zacher, B.; Gantz, J. L.; Richards, R. E.; Armstrong, N. R. Organic Solar Cells—At the Interface. *J. Phys. Chem. Lett.* **2013**, *4*, 1949−1952.

(13) Street, R. A.; Krakaris, A.; Cowan, S. R. Recombination through Different Types of Localized States in Organic Solar Cells. *Adv. Funct. Mater.* **2012**, *22*, 4608−4619.

(14) Ratcliff, E. L.; Garcia, A.; Paniagua, S. A.; Cowan, S. R.; Giordano, A. J.; Ginley, D. S.; Marder, S. R.; Berry, J. J.; Olson, D. C. Investigating the Influence of Interfacial Contact Properties on Open Circuit Voltages in Organic Photovoltaic Performance: Work Function versus Selectivity. *Adv. Energy Mater.* **2013**, *3*, 647−656.

(15) Hotchkiss, P. J.; Li, H.; Paramonov, P. V.; Paniagua, S. A.; Jones, S. C.; Armstrong, N. R.; Brédas, J.-L.; Marder, S. R. Modification of the Surface Properties of Indium Tin Oxide with Benzylphosphonic Acids: A Joint Experimental and Theoretical Study. *Adv. Mater.* **2009**, *21*, 4496−4501.

(16) Song, C. K.; White, A. C.; Zeng, l.; Leever, B. J.; Clark, M. D.; Emery, J. D.; Lou, S. J.; Timalsina, A.; Chen, L. X.; Bedzyk, M. J.; Marks, T. J. Systematic Investigation of Organic Photovoltaic Cell Charge Injection/Performance Modulation by Dipolar Organosilane Interfacial Layers. *ACS Appl. Mater. Interfaces* **2013**, *5*, 9224−9240.

(17) Ratcliff, E. L.; Zacher, B.; Armstrong, N. R. Selective Interlayers and Contacts in Organic Photovoltaic Cells. *J. Phys. Chem. Lett.* **2011**, *2*, 1337−1350.

(18) Steim, R.; Kogler, F. R.; Brabec, C. J. Interface Materials for Organic Solar Cells. *J. Mater. Chem.* **2010**, *20*, 2499−2512.

(19) Vasilopoulou, M.; Georgiadou, D. G.; Douvas, A. M.; Soultati, A.; Constantoudis, V.; Davazoglou, D.; Gardelis, S.; Palilis, L. C.; Fakis, M.; Kennou, S.; et al. Porphyrin Oriented Self-Assembled Nanostructures for Efficient Exciton Dissociation in High-Performing Organic Photovoltaics. *J. Mater. Chem. A* **2014**, *2*, 182−192.

(20) Vasilopoulou, M.; Douvas, A.M.; Georgiadou, D. G.; Constantoudis, V.; Davazoglou, D.; Kennou, S.; Palilis, L. C.; Daphnomili, D.; Coutsolelos, A. G.; Argitis, P. Large Work Function Shift of Organic Semiconductors Inducing Enhanced Interfacial Electron Transfer in Organic Optoelectronics Enabled by Porphyrin Aggregated Nanostructures. *Nano Res.* **2014**, DOI: 10.1007/s12274-014-0428-9.

(21) Graetzel, M.; Janssen, R. A. J.; Mitzi, D. B.; Sargent, E. H. Materials Interface Engineering for Solution-processed Photovoltaics. *Nature* **2012**, *488*, 304−312.

(22) Steirer, K. X.; Ndione, P. F.; Widjonarko, N. E.; Lloyd, M. T.; Meyer, J.; Ratcliff, E. L.; Kahn, A.; Armstrong, N. R.; Curtis, C. J.; Ginley, D. S.; et al. Enhanced Efficiency in Plastic Solar Cells via Energy Matched Solution Processed NiO_x Interlayers. *Adv. Energy Mater.* **2011**, *1*, 813−820.

(23) Greiner, M. T.; Chai, L.; Helander, M. G.; Tang, W.-M.; Lu, Z.-H. Transition Metal Oxide Work Functions: The Influence of Cation Oxidation State and Oxygen Vacancies. *Adv. Funct. Mater.* **2012**, *22*, 4557−4568.

(24) Greiner, M. T.; Helander, M. G.; Tang, W.-M.; Wang, Z.-B.; Qiu, J.; Lu, Z.-H. Universal Energy-Level Alignment of Molecules on Metal Oxides. *Nat. Mater.* **2012**, *11*, 76−81.

(25) Greiner, M. T.; Lu, Z.-H. Thin-Film Metal Oxides in Organic Semiconductor Devices: Their Electronic Structures, Work Functions and Interfaces. *NPG Asia Mater.* **2013**, *5*, e55.
(26) Zhang, Z.; Xiao, Y.; Wei, H.-X.; Ma, G.-F.; Duhm, S.; Li, Y.-Q.; Tang, J.-X. Impact of Oxygen Vacancy on Energy-Level Alignment At MoOx/Organic Interfaces. *Appl. Phys. Express* **2013**, *6*, 095701.
(27) Hancox, I.; Chauhan, K. V.; Sullivan, P.; Hatton, R. A.; Moshar, A.; Mulcahy, C. P. A.; Jones, T. S. Increased Efficiency of Small Molecule Photovoltaic Cells by Insertion of a MoO_3 Hole-Extracting Layer. *Energy Environ. Sci.* **2010**, *3*, 107−110.
(28) Vasilopoulou, M.; Douvas, A. M.; Georgiadou, D. G.; Palilis, L. C.; Kennou, S.; Sygellou, L.; Soultati, A.; Kostis, I.; Papadimitropoulos, G.; Davazoglou, D.; et al. The Influence of Hydrogenation and Oxygen Vacancies on Molybdenum Oxides Work Function and Gap States for Application in Organic Optoelectronics. *J. Am. Chem. Soc.* **2012**, *134*, 16178−16187.
(29) Vasilopoulou, M.; Soultati, A.; Georgiadou, D. G.; Palilis, L. C.; Kennou, S.; Stathopoulos, N. A.; Davazoglou, D.; Argitis, P. Hydrogenated Under-Stoichiometric Tungsten Oxide Anode Interlayers for Efficient and Stable Organic Photovoltaics. *J. Mater. Chem. A* **2014**, *2*, 1738−1749.
(30) Vasilopoulou, M.; Palilis, L. C.; Georgiadou, D. G.; Kennou, S.; Kostis, I.; Davazoglou, D.; Argitis, P. Barrierless Hole Injection through Sub-Bandgap Occupied States in Organic Light Emitting Diodes Using Substoichiometric MoO(x) Anode Interfacial Layer. *Appl. Phys. Lett.* **2012**, *100*, 13311.
(31) Braun, S.; Salaneck, W. R.; Fahlman, M. Energy-Level Alignment at Organic/Metal and Organic/Organic Interfaces. *Adv. Mater.* **2009**, *21*, 1450−1472.
(32) Irfan; Ding, H.; Gao, Y.; Small, C.; Kim, D. Y.; Subbiah, J.; So, F. Energy Level Evolution of Air and Oxygen Exposed Molybdenum Trioxide Films. *Appl. Phys. Lett.* **2010**, *96*, 243307.
(33) Meyer, J.; Shu, A.; Kröger, M.; Kahn, A. Effect of Contamination on the Electronic Structure and Hole-Injection Properties of MoO_3/Organic Semiconductor Interfaces. *Appl. Phys. Lett.* **2010**, *96*, 133308.
(34) Irfan, I.; Turinske, A. J.; Bao, Z.; Gao, Y. Work Function Recovery of Air Exposed Molybdenum Oxide Thin Films. *Appl. Phys. Lett.* **2012**, *101*, 093305.
(35) Papadimitropoulos, G.; Vourdas, N.; Giannakopoulos, K.; Vasilopoulou, M.; Davazoglou, D. Poroous Hot-Wire Deposited WO_3 Films with High Optical Transmission. *J. Appl. Phys.* **2011**, *109*, 103527.
(36) Vourdas, N.; Papadimitropoulos, G.; Kostis, I.; Vasilopoulou, M.; Davazoglou, D. Substoichiometric Hot-Wire WO_x Films Deposited in Reducing Environment. *Thin Solid Films* **2012**, *520*, 3614−3619.
(37) Kostis, I.; Vourdas, N.; Vasilopoulou, M.; Douvas, A. M.; Papadimitropoulos, G.; Konofaos, N.; Iliadis, A.; Davazoglou, D. Formation of Stoichiometric, Sub-Stoichiometric Undoped and Hydrogen Doped Tungsten Oxide Films, enabled by Pulsed Introduction of O2 or H2 during Hot-Wire Vapor Deposition. *Thin Solid Films* **2013**, *537*, 124−130.
(38) Vasilopoulou, M.; Papadimitropoulos, G.; Palilis, L. C.; Georgiadou, D. G.; Argitis, P.; Kennou, S.; Kostis, I.; Vourdas, N.; Stathopoulos, N. A.; Davazoglou, D. High Performance Organic Light Emitting Diodes Using Substoichiometric Tungsten Oxide As Efficient Hole Injection Layer. *Org. Electron.* **2012**, *13*, 796−806.
(39) Kostis, I.; Vourdas, N.; Papadimitropoulos, G.; Douvas, A. M.; Vasilopoulou, M.; Boukos, N.; Davazoglou, D. Effect of the Oxygen Substoichiometry and of Hydrogen Insertion on the Formation of Intermediate Bands within the gap of Disordered Molybdenum Oxide Films. *J. Phys. Chem. C* **2013**, *117*, 18013−18020.
(40) Clark, D. E.; Sutton, W. H. Microwave Processing of Materials. *Annu. Rev. Mater. Sci.* **1996**, *26*, 299−331.
(41) Bykov, Y. V.; Rybakov, K. I.; Semenov, V. E. High-Temperature Microwave Processing of Materials. *J. Phys. D: Appl. Phys.* **2001**, *34*, R55.
(42) Paine, D. C.; Yeom, H.-Y.; Yaglioglu, B. Transpardent Conducting Oxide Materials and Technology. *Flexible Flat Panel Displays*; Crawford, G., Ed.; John Wiley and Sons: Chichester, U.K., 2005
(43) MacDiarmid, A. G. Synthetic Metals: A Novel Role for Organic Polymers. *Synth. Met.* **2002**, *125*, 11−22.
(44) Sumana, K. S.; Rao, K. N.; Krishna, M.; Murthy, C. S. C.; Rao, Y. V. S.; Phani, A. R. Structural and Electrical Properties of the Microwave Irradiated and Conventionally Annealed TiO_2 Thin Films Derived from Sol-Gel Process. *Int. J. Eng. Res. Appl.* **2012**, *2*, 681−686.
(45) Jeong, S.; Moon, J. Low-Temperature, Solution-Processed Metal Oxide Thin Film Transistors. *J. Mater. Chem.* **2012**, *22*, 1243−1250.
(46) Palilis, L. C.; Vasilopoulou, M.; Georgiadou, D. G.; Argitis, P. A Water Soluble Inorganic Molecular Oxide as a Novel Efficient Electron Injection Layer for Hybrid Light-Emitting Diodes (HyLEDs). *Org. Electron.* **2010**, *11*, 887−894.
(47) Palilis, L. C.; Vasilopoulou, M.; Douvas, A. M.; Georgiadou, D. G.; Kennou, S.; Stathopoulos, N. A.; Constantoudis, V.; Argitis, P. Solution Processable Tungsten Polyoxometalate as Highly Effective Cathode Interlayer for Improved Efficiency and Stability Polymer Solar Cells. *Sol. Energy Mater. Sol. Cells* **2013**, *114*, 205−213.
(48) He, Z.; Zhong, C.; Huang, X.; Wong, W.-Y.; Wu, H.; Chen, L.; Su, S.; Cao, Y. Simultaneous Enhancement of Open-Circuit Voltage, Short-Circuit Current Density, and Fill Factor in Polymer Solar Cells. *Adv. Mater.* **2011**, *23*, 4636−4643.
(49) Lampert, M. A.; Mark, P. *Current Injection in Solids*; Academic Press: New York, 1970.
(50) Boix, P. P.; Garcia-Belmonte, G.; Munecas, U.; Neophytou, M.; Waldauf, C.; Pacios, R. Determination of Gap Defect States in Organic Bulk Heterojunction Solar Cells from Capacitance Measurements. *Appl. Phys. Lett.* **2009**, *95*, 233302.
(51) Knesting, K. M.; Ju, H.; Schlenker, C. W.; Giordano; Garcia, A.; Smith; O'Neil, L.; Olson, D. C.; Marder, S. R.; Ginger, D. S. ITO Interface Modifiers Can Improve V_{oc} in Polymer Solar Cells and Suppress Surface Recombination. *J. Phys. Chem. Lett.* **2013**, *4*, 4038−4044.
(52) Groves, C.; Marsh, R. A.; Greenham, N. C. Monte Carlo Modeling of Geminate Recombination in Polymer−Polymer Photovoltaic Devices. *J. Chem. Phys.* **2008**, *129*, 114903.